Synthesis, Kinetics, and Structural Studies of a Photolabile Caged Isocitrate: A Catalytic Trigger for Isocitrate Dehydrogenase†

Michael J. Brubaker,‡ David H. Dyer,§ Barry Stoddard,§ and Daniel E. Koshland, Jr.*,||

Center for Advanced Materials, Lawrence Berkeley Laboratory, and Department of Molecular and Cell Biology, Stanley Hall, University of California, Berkeley, California 94720, and Division of Basic Sciences, Program in Structural Biology, Fred Hutchinson Cancer Research Center, 1124 Columbia Street, Seattle, Washington 98104

Received May 16, 1995; Revised Manuscript Received November 15, 1995⊗

ABSTRACT: A biologically inactive photolabile derivative of isocitrate has been synthesized and characterized. The caged isocitrate is photolyzed to isocitrate with a rate constant of 234 s^{-1}, a half-life of 3 ms, and a quantum yield of 0.3 at pH = 6.4. Caged isocitrate (1-(2-nitrophenyl)ethyl 1-hydroxy-1,2-dicarboxy-3-propanecarboxylate) was synthesized in a straightforward synthetic manner starting with racemic isocitric acid lactone. Laser pulse photolysis at a wavelength of 355 nm was used to determine the rate of photolysis and the quantum yield and to quantify the amount of energy needed for quantitative conversion of the caged isocitrate to free isocitrate. Enzymatic conversion of the liberated isocitrate to α-ketoglutarate was achieved in solution as well as in wild-type and mutant isocitrate dehydrogenase (IDH) protein crystals. The X-ray crystal structures of wild-type IDH soaked with photolabile caged isocitrate and Mg^{2+} and void of nicotinamide adenine dinucleotide phosphate were solved at 2.5 Å resolution before and after photolysis and compared by difference mapping against previously determined enzyme structures. Prior to photolysis the enzyme active site contains a low occupancy of bound free Mg^{2+} in the metal binding site but no observable bound isocitrate, whereas after photolysis the enzyme is complexed to liberated isocitrate and Mg^{2+} with binding interactions identical to those of previously determined substrate complexes. Single-crystal spectroscopy of the crystals after flash photolysis in the presence of substrates shows production of bound enzyme−substrate complexes and reduced nicotinamide adenine dinucleotide phosphate induced by the photolytic event.

The use of photolabile (caged) compounds has enabled investigators to control the rapid release of biological important effectors within intact biological systems [reviews by Corrie and Trentham (1993) and McCray and Trentham (1989)]. An emerging and very important application of caged effectors is to aid in the capture and observation of catalytic intermediates in protein crystals using the time-resolved techniques of Laue X-ray crystallography (Moffat, 1989; Hadju & Johnson, 1990; Cruickshank et al., 1992). The uses of caged effectors have allowed researchers to initiate reactions catalyzed by crystalline proteins rapidly and uniformly (Schlichting et al., 1989; Stoddard et al., 1991; Duke et al., 1992). Caged effectors are biologically inactive, which circumvents the problems of diffusion, degradation, and desensitization of the biological response (Gurney & Lester, 1987) normally associated with trying to measure or observe time-resolved processes with biologically active effectors.

There have been numerous biological compounds altered in various ways rendering them biologically inactive and photolabile. The most successful and most common photolabile moiety is the 2-nitrobenzyl group that has been effectively used to cage biologically important molecules such as neurotransmitters and amino acids, nucleotides, nucleotide analogs, and other phosphate esters, and calcium chelators [reviewed in McCray and Trentham (1989) and Adams and Tsien (1993)]. The 2-nitrobenzyl moiety has the important advantages of compatibility with a wide variety of functional groups, ease of synthesis, stability, low light sensitivity, and a high rate of photolysis (Adams & Tsien, 1993).

This study involves the synthesis, characterization, photolysis, kinetics, quantum yield, stability, and biological activity in solution and in protein crystals of caged isocitrate. X-ray crystallography structure determinations of isocitrate dehydrogenase complexes produced by flash photolysis of caged isocitrate are also presented.

Isocitrate dehydrogenase (*Escherichia coli*) catalyzes the oxidation and decarboxylation of isocitrate to α-ketoglutarate. The postulated mechanism (Stryer, 1988) is thought to occur in two distinct steps with oxidation preceding decarboxylation of the oxalosuccinate intermediate:[1]

† Support was obtained from the Center for Advanced Materials, Lawrence Berkeley Laboratory, for D.E.K. and M.J.B., from NIH Grant R01-GM49857 for B.L.S., and from NSF for D.E.K.

‡ Lawrence Berkeley Laboratory, University of California.

§ Fred Hutchinson Cancer Research Center.

|| Department of Molecular and Cell Biology, University of California.

⊗ Abstract published in *Advance ACS Abstracts,* February 1, 1996.

[1] Abbreviations: IDH, isocitrate dehydrogenase (*Escherichia coli*); DMAP, (dimethylamino)pyridine; DCC, 1,3-dicyclohexylcarbodiimide; THF, tetrahydrofuran; DMF, dimethylformamide; $CHCl_3$, chloroform; CH_2Cl_2, methylene chloride; EtOAc, ethyl acetate; TLC, thin layer chromatography; HPLC, high-performance liquid chromatography; TMS, tetramethylsilane; NMR, nuclear magnetic resonance; IR, infrared spectra; HRMS, high-resolution mass spectrometry; FAB, fast atom bombardment; $NADP^+$, nicotinamide adenine dinucleotide phosphate; NADPH, reduced nicotinamide adenine dinucleotide phosphate; MTT, thiazolyl blue; PES, phenazine ethosulfate; G6P, glucose 6-phosphate; G6PD, glucose-6-phosphate dehydrogenase.

0006-2960/96/0435-2854$12.00/0

$$\text{isocitrate}^{3-} + \text{NADP}^{+} + \text{Mg}^{2+} \leftrightarrow [\text{oxalosuccinate}^{3-}] + \text{NADPH} + \text{H}^{+}$$

$$[\text{oxalosuccinate}^{3-}] + \text{H}^{+} + \text{Mg}^{2+} \leftrightarrow \alpha\text{-ketoglutarate}^{2-} + \text{CO}_2$$

Direct observation of enzyme substrate intermediates such as oxalosuccinate has long been the goal of many researchers but has been very difficult to achieve. Thus, through the combined techniques of flash photolysis of photolabile caged isocitrate and Laue X-ray crystallography, it might be possible to observe the oxalosuccinate intermediate in real time.

EXPERIMENTAL PROCEDURES

Unless otherwise noted, all materials were obtained from commercial suppliers and used without further purification. DMF was dried sequentially over 4 Å molecular sieves. Isocitric acid lactone, DMAP, and DCC were dried in vacuo over phosphorous pentoxide. Reactions and chromatography fractions were analyzed with Analtech 250 μm Silica Gel GF plates.

Melting points were determined with a capillary melting point apparatus (Thomas Hoover) and are uncorrected. Infrared spectra were recorded on a Nicolet 5DX FT infrared spectrophotometer. High-performance liquid chromatography was performed with a Waters model 688 auto gradient controller, model 510 pump, model U6K injector, model 441 absorbance detector, and Omniscribe D-5000 strip chart recorder. Enzymatic assays utilizing UV monitoring were performed using a Hewlett-Packard model 8452A diode array spectrophotometer.

^{1}H NMR spectra were determined at 400 or 500 MHz on Bruker superconducting FT spectrometers. Chemical shifts are reported in δ values, positive values indicating shifts downfield from tetramethylsilane. Fast atom bombardment (FAB+) mass spectra were recorded at the University of California Berkeley Mass Spectral Laboratory on an AE1 M512 mass spectrometer. Mass spectral data are reported as *m*/*z* for the molecular ion. Elemental analyses were performed by the Microanalytical Laboratory, operated by the College of Chemistry, University of California (Berkeley, CA).

Synthesis

*Di-tert-butyl 2-Oxotetrahydrofuran-4,5-dicarboxylate (**I**).* Isocitric acid lactone (1.74 g, 10 mmol), DMAP (0.122 g, 1 mmol), and *tert*-butyl alcohol (5.92 g, 80 mmol) were dissolved in 20 mL of anhydrous DMF under a nitrogen atmosphere and then cooled to 0−5 °C with vigorous stirring. DCC (4.33 g, 21 mmol) was added in one portion, and the resulting clear solution was stirred vigorously for 5 min at 0−5 °C. Precipitating urea appeared within 2−3 min after addition of the DCC. After 5 min the ice bath was removed, and the reaction was warmed to room temperature and stirred for 1.5 h. Upon warming to room temperature, the solution became colored from red to deep purple with a heavy precipitate. The solution was filtered, the filter cake was washed thoroughly with DMF, and the solvent was removed in vacuo. The remaining dark colored oil was taken up in CH_2Cl_2 and filtered to remove any precipitate, and the solvent was removed in vacuo to remove any traces of DMF. The resulting oil was taken up again in CH_2Cl_2 and washed with 0.1 N HCl (3 × 100 mL), the aqueous washings were back extracted (2 × 25 mL) with CH_2Cl_2, and the organic layers were combined. The combined organic layers were washed with saturated $NaHCO_3$ (three times with 50 mL) and brine (one time with 50 mL) and dried over anhydrous Na_2SO_4. The solvent was removed to yield a purple colored oil (2.0 g, 71%). The oil was taken up in a minimum of CH_2Cl_2 and loaded onto a 3 × 17 cm flash chromatography column containing silica gel (Aldrich, Merck grade 9385) and eluted with CH_2Cl_2. The product was obtained as a pure oil which solidified upon standing at 5 °C (1.19 g, 42%). If desired, the product can be recrystallized from warm hexane: ^{1}H NMR ($CDCl_3$, TMS) δ 4.95 (d, 1H), 3.3 (m, 1H), 2.8 (d, 2H), 1.5 (s, 9H), 1.48 (s, 9H); IR (KBr, cm^{-1}) 1800, 1746; mp 44−45 °C. Anal. Calcd for $C_{14}H_{22}O_6$: C, 58.74; H, 7.69. Found: C, 58.79, H, 7.47.

*Di-tert-butyl 1-Hydroxy-3-carboxy-1,2-propanedicarboxylate-3 (**II**).* Compound **I** (1.19 g, 4.2 mmol) was suspended in an equal molar amount of 0.1 N NaOH and placed in a 65 °C oil bath with stirring for 10 min. The suspended material dissolved completely within 2 min. The reaction flask was immediately placed on ice for 10 min. The cooled solution was extracted with CH_2Cl_2 (2 × 20 mL), acidified with 1 N HCl to pH = 3, and then extracted with CH_2Cl_2 (4 × 20 mL). The combined CH_2Cl_2 layers were dried over anhydrous Na_2SO_4. Evaporation of the solvent left behind 460 mg (37%) of a clear oil which solidified upon cooling. The product obtained in this way is analytically pure and does not require further purification: ^{1}H NMR ($CDCl_3$, TMS) δ 4.5 (d, 1H), 3.22 (m, 1H), 2.9 (dd, 1H), 2.25 (dd, 1H), 1.5 (s, 9H), 1.47 (s, 9H); mp 66−68 °C; IR (KBr, cm^{-1}) 3494, 1734. Anal. Calcd for $C_{14}H_{24}O_7$: C, 55.24; H, 7.89. Found: C, 55.22; H, 7.76.

*1,2-Di-tert-butyl 3-(1-(2-Nitrophenyl)ethyl 1-Hydroxy-1,2,3-propanetricarboxylate (**III**).* The hydrazone of 2-nitroacetophenone was prepared by the method described by Walker et al. (1988). The hydrazone of 2-nitroacetophenone (2.63 g, 14.7 mmol) was dissolved in 20 mL of $CHCl_3$ in a foil-covered round bottom flask. Manganese dioxide (14.7 g, 169 mmol) was added cautiously to the vigorously stirred solution. The suspension was stirred in the dark for 30 min at room temperature. The solution was then filtered through a Celite pad directly into a stirred solution of **II** (0.547 g, 1.8 mmol) in 10 mL of CH_2Cl_2. The Celite pad was washed with $CHCl_3$ until the pad was free of the red-colored diazo compound. Nitrogen gas evolution was observed immediately upon addition of the diazo compound, and the red color rapidly faded upon the initial addition; however, the red color persisted upon complete addition. The red-colored solution was protected from light and stirred vigorously for 48 h at room temperature. After the prescribed reaction time, the solution was filtered through a short plug of silica gel to destroy any remaining diazo compound. The plug was washed with $CHCl_3$, and the solvent was removed in vacuo to yield a yellow-colored oil. The desired product proved to be difficult to separate chromatographically. The following method was repeatable with crude product amounts of up to 600 mg. The oil was taken up in a minimum of CH_2Cl_2 and loaded onto a flash chromatography silica gel (Aldrich, Merck grade 9385) column (1 × 18 cm) and eluted with 200 mL of CH_2Cl_2 followed by 100 mL of 10% EtOAc

in CH_2Cl_2. Fractions (2−3 mL) were collected and analyzed by TLC (same eluting solvent). The product actually exhibits a greater R_f on TLC but is contained in a latter fraction from the column. The fractions that contained the product were combined, and the solvent was removed in vacuo to yield 0.54 g (66%) of pure product as a yellow-colored oil: ^{1}H NMR ($CDCl_3$, TMS) δ 7.93 (m, 1H), 7.69 (m, 2H), 7.43 (m, 1H), 6.35 (m, 1H), 4.47 (d, 1H), 3.22 (m, 1H), 2.88 (m, 1H), 2.23 (m, 1H), 1.65 (dd, 3H), 1.45 (m, 18H); IR (KBr, cm^{-1}) 3502, 1746, 757. Anal. Calcd for $C_{22}H_{31}NO_9$: C, 58.28; H, 6.84; N, 3.09. Found: C, 58.54; H, 6.96; N, 3.28.

*1-(2-Nitrophenyl)ethyl 1-Hydroxy-1,2-dicarboxy-3-propanecarboxylate (**IV**) ("caged isocitrate").* In a foil-covered flask 10 mL of freshly distilled TFA was mixed with **III** (0.460 g, 1.02 mmol) under a nitrogen atmosphere. The solution was stirred at room temperature for 15 min. The solvent was removed in vacuo, and the brown-colored oil was taken up in 8 mL of 5% $NaHCO_3$. The aqueous solution was extracted with EtOAc (6 × 2 mL) and then acidified with 1 N HCl to pH 1. The resulting cloudy solution was extracted with EtOAc (5 × 3 mL), readjusted to pH 1, and extracted again with EtOAc (2 × 3 mL). The combined organic fractions were dried over anhydrous Na2SO4, and the solvent was removed in vacuo to yield 0.24 g (69%) of crude product. The crude material was dissolved in a minimum of 1:1 CH_2Cl_2:EtOAc chilled on ice, an equal volume of hexane was added, and the solution was cooled to −20 °C. Upon standing at −20 °C overnight the product crystallized. The crystals were collected and dried in vacuo to yield 0.133 g (38%) of pure product: ^{1}H NMR (acetone-d_6, TMS) 7.95 (m, 1H), 7.78 (m, 2H), 7.55 (m, 1H), 6.2 (m, 1H), 4.7 (m, 1H), 3.35 (m, 1H), 2.93 (m, 1H), 2.9 (br, 1H), 2.44 (m, 1H), 1.6 (d, 3H); mp 138−139 °C; IR (KBr, cm^{-1}) 3526, 1736, 755. HRMS (FAB, MH^+) calculated for $C_{14}H_{16}N_1O_9$ 342.082506, found 342.083430.

The purity of **IV** was determined by HPLC using a Biorad aminex HPX-87H column. Isocratic elution of the compound was accomplished with 5 mM H_2SO_4 at a flow rate of 0.5 mL/min. The effluent was monitored at 214 and 254 nm. A 5 μL injection of **IV** (0.2 mM) gave only one peak with a retention time of 96.5 min at 214 nm, while a 5 μL (0.2 mM) injection of a standard sample of D,L-isocitrate gave a spectra consisting of two peaks at 10.8 and 23.8 min, respectively. The same injections monitored at 254 nm resulted in only one peak being observed for **IV** (retention time of 86.3 min), and no peaks were observed for D,L-isocitrate. The retention time differences for **IV** between the two observed wavelengths is due to different batches of eluting solvent.

Kinetic Assays

Isocitrate Dehydrogenase Activity Assay. Compound **IV** was directly assayed at 25 °C for substrate activity using 100 mM Tris buffer pH 7.81, 0.01 M $MgCl_2$, 68 ng of IDH, 5 μM (or 5 mM) **IV**, and 0.2 mM $NADP^+$. The assays were initiated by the addition of $NADP^+$. The assays were monitored by directly measuring the production of NADPH by determining the OD_{340} at 240 s in 1 cm semimicro disposable cuvettes. The concentration of NADPH was determined using a molar extinction coefficient of 6270 M^{-1} cm^{-1}. The data obtained is expressed as a percentage of the activity ($NADP^+$ production) obtained when using equivalent amounts of D,L-isocitrate as the substrate. At t = 240 s the catalysis is complete, and there is no appreciable change in the OD_{340} of the sample. The assays were repeated at least three times.

Isocitrate Dehydrogenase Activity Coupled to Glucose-6-phosphate Dehydrogenase Assay. When the IDH reaction is coupled to a G6PD assay system, it is possible to measure picomole levels of NADPH (Bernofsky & Swan, 1973; Nisselbaum & Green, 1969).

Incubation Mix (A). In a 1.5 mL eppendorf tube 100 mM Tris buffer pH 7.81, 10 mM $MgCl_2$, 200 μM D,L-isocitrate or 200 μM compound **IV**, 200 μM $NADP^+$, and 925 ng of IDH were combined. The reaction was initiated by the addition of IDH.

Alkaline Mix (B). At t = 10 min a 80 μL aliquot of incubation mix A was mixed with 120 μL of 1.0 N NaOH and heated for 2 min at 85−90 °C to destroy any remaining $NADP^+$. The sample was immediately neutralized by the addition of 22.5 μL of 5 N HCl and placed on ice. The pH was checked periodically to ensure the solution was neutral.

Assay Mix (C). To a solution containing 0.52 μmol of MTT, 2.0 μmol of PES, 7.5 μmol of G6P, 57 mM glycylglycine buffer pH 7.4 containing 57 mM nicotinamide, and 24.4 U of G6PD, 200 μL of the neutralized alkaline mix B was added and mixed thoroughly, and the absorbance was measured at 570 nm for at least 60 s.

The blank rate was determined by using the above mixture of components in assay mix C except that water was used in the place of G6PD. The control consisted of the above mixtures (assay mixes A, B, and C) in which D,L-isocitrate was used in place of **IV** in assay mix A. All steps were conducted at 25 °C unless otherwise indicated. The results reported are the average of at least three trials.

To determine the minimum level of NADPH that could be reliably detected, a NADPH standard curve was constructed using the above method except that in incubation mix A, IDH was excluded and known amounts of NADPH were added in place of $NADP^+$.

Laser Pulse Photolysis and Spectroscopy

Quantum Yield. The samples were excited with single pulses (10 ns, 25 mJ) delivered from a frequency-tripled Quantel YG481 Nd:YAG laser. Incident laser intensities were attenuated with crossed polarizers and defocused onto the sample cell. Solutions were adjusted to possess an absorbance of 0.20 at 355 nm and were purged continuously with N_2. Laser intensities were calibrated using zinc *meso*-tetraphenylporphyrin in benzene as a standard for which the triplet quantum yield (Hurley et al., 1983) was taken to be 0.83 and the molar differential extinction coefficient (Pekkarinen & Linschitz, 1960) at 470 nm was taken as 74 000 M^{-1} cm^{-1}. Transient differential absorption spectra were recorded point-by-point with 5 individual laser shots being averaged at each wavelength. Formation of the *aci*-nitro intermediate (Figure 2) was monitored at 410 nm using a molar differential extinction coefficient (Walker et al., 1988) of 9100 M^{-1} cm^{-1}. The initial absorbance at 410 nm was determined by computer extrapolation to the center of the laser pulse for a series of incident laser intensities and with 20 individual laser shots being averaged for each determination. Identical measurements were made for formation of the zinc porphyrin triplet excited state, at 470

nm, so that the quantum yield for formation of the *aci*-nitro intermediate could be derived. These experiments were repeated at several different pH values.

Decay Kinetics. Decay of the *aci*-nitro derivative was monitored at 410 nm following excitation at 355 nm with a 10 ns laser pulse. Solutions were adjusted to the required pH and purged continuously with N_2 during the experiment. The monitoring beam was provided with a stabilized 15 W tungsten lamp. Approximately 100 individual laser shots were averaged, and the corresponding base lines (recorded without laser excitation) were subtracted for each measurement. Kinetic analysis was made by nonlinear, least-squares computer iteration. To avoid problems from photolysis of **IV**, the solution was flowed through the sample cell, and the monitoring beam was passed through a 410 nm narrow band-pass filter positioned before the cell. The experiment was repeated four times.

Solution Flash Photolysis in the Presence of Enzyme. Kinetics of the flash photolysis of **IV** in the presence of IDH employed the following conditions: Tris buffer pH 7.8 (0.1 M), $MgCl_2$ (0.01 M), compound **IV** (1.85 mM), $NADP^+$ (2.0 mM), IDH (194 μg), and water to give a final volume of 2 mL. The increase in absorbance at 340 nm was monitored following laser excitation (10 ns pulses, 25 mJ/pulse) at 355 nm after deoxygenation of the solution by purging with N_2. A sample of the same solution not containing IDH was used as a control. The pH was checked after addition of all the ingredients and was found to be 7.81. After laser excitation, absorbance changes were monitored at 340 and at 410 nm. After computer normalization of the signal at 410 nm, as observed in the absence and presence of IDH, the signal obtained at 340 nm in the absence of IDH was used to correct the base line for the sample containing IDH.

*Quantitation of the Isocitrate Released from **IV**.* Experiments were made with a 2 mL aliquot of solution containing 3.6×10^{-7} mol of **IV** in buffer (0.1 M Tris, pH 7.8). The solution was irradiated with a single laser pulse, and the initial absorbance due to the *aci*-nitro intermediate was measured at 410 nm. This procedure was repeated until no further absorbance change could be observed and the individual absorbance values were summed. The molar extinction coefficient of 9100 M^{-1} cm^{-1} at 410 nm for the *aci*-nitro intermediate was used to calculate the amount of isocitrate released upon illumination.

Crystallographic Studies

Data Collection and Photolysis in the Crystal. Isocitrate dehydrogenase was purified (Reeves et al., 1972; LaPorte et al., 1985) and crystallized (Hurley et al., 1989; Stoddard et al., 1992) as described previously. The crystals were 0.5−1.5 mm per side, space group $P4_32_12$. The unit cell dimensions prior to photolysis and after binding liberated substrate consistently refined to values within 0.5% of the previously published lengths during data processing (Table 1).

A large (1.2 mm) crystal was transferred to a 0.5 mL volume of a stabilization solution (generally 10% higher ammonium sulfate than that used to grow the crystals, buffered at pH 8.0 with Tris-HCl), and soaked overnight in the dark with 80 mM compound **IV** and magnesium sulfate. To protect the crystal from oxidative degradation after photolysis by liberated nitrosoketone (Figure 2), β-mercaptoethanol (10 mM) and dithiothreitol (10 mM) were also added to the mother liquor. To avoid catalytic turnover, $NADP^+$ was not a constituent of the mother liquor. The crystal was mounted under safe-light in quartz capillaries with mother liquor at either end of the capillary. The mount was sealed with mineral oil and paraffin wax. Initial data were collected at room temperature in the dark on an R-axis imaging plate area detector with a Rigaku RU-200 rotating anode X-ray generator operating at 50 kV, 80 mA. A complete data set was collected from this crystal to 2.5 Å resolution using 20 1.5° rotations at 30 min/deg, followed by an additional seven frames collected with the crystal on a 45° jig (Molecular Structure Corporation) for completeness. The total decay after collection of this data set was less than 5% of the initial structure average factor amplitudes. The crystal was then irradiated for 2 min with a Cole Parmer 9741-50 quartz halogen light source with a 9741-03 high-intensity 150 W bulb and dual fiber optic light pipes and focusing lenses. The crystal was irradiated from two directions simultaneously, 90° apart in order to maximize efficient excitation of **IV** in the crystal lattice. A second data set was then collected after photolysis with an identical strategy to that described above.

Table 1: Data Processing and Refinement Statistics

data set	dark	after photolysis
exposure time (h)	8	8
rotations (deg)	30 × 1.5	30 × 1.5
radiation-induced decay (%)	5	4 (9 total for crystal)
total unique reflections	21 403	20 683

	dark		after photolysis	
	overall	2.75−2.5 Å	overall	2.75−2.5 Å
R_{symm}[a] (%)	6.24	12.4	6.38	13.2
resolution (Å)	2.5		2.5	
$R_{refinement}$[b] (%)	18.1	27.0	18.8	27.9
R_{iso}[c] (%)			12.2	

structural statistics	dark	after photolysis
total atoms	3870	3881
bond distance rms (Å)	0.014	0.015
bond angle rms (deg)	2.8	2.7
dihedral rms (deg)	24.3	23.8

[a] R_{symm} = initial overall R-factor (on intensities) between all symmetry related reflections in the final merged data set. $R = \sum_j(I_1(j) - I_2(j))/\sum_j(I(j))$. [b] $R_{refinement} = \sum_j|(F_{obs}(j) - F_{calc}(j))|/\sum_j(F_{obs}(j))$. [c] R_{iso} = overall agreement between data sets shown above after applying single global scale factor. $R = \sum_j(I_1(\text{dark}) - I_2(\text{light}))/\sum_j(I(\text{dark}))$.

For both data sets, a 2.0σ cutoff was applied on intensities, followed by rejection of all reflections with structure factor amplitudes less than one-third the average value of F for the overall data set (approximately 5% of the total reflections processed). For both data sets, over 85% of the unique data were present in the final data set. The internal merging R_{symm} for each crystal and overall R_{merge} between crystals for each individual data set are shown in Table 1 and compare favorably with past reported IDH structure determinations (Hurley et al., 1989, 1990a, 1990b, 1991; Stoddard et al., 1993a, 1993b). The data collection software package R-axis (Molecular Structure Corporation) was used to collect and process the data, and protein difference Fourier maps were calculated using the software package PROTSYS.

In order to assess the presence of bound isocitrate or its caged precursor (**IV**) in the enzyme active site prior to photolysis, difference Fourier syntheses with the coefficients

$[F_{o(\text{soaked crystals, dark})} - F_{c(\text{apoenzyme, wild-type})}]\alpha_{calc}$ were calculated using the experimentally determined structure factor amplitudes for the soaked enzyme prior to irradiation and for the apoenzyme in the absence of **IV**. Initial phases were calculated with the coordinates of wild-type apoenzyme (Hurley et al., 1989) from the Brookhaven PDB (Bernstein et al., 1977) as the initial model (accession number 3ICD). These maps were examined using the program QUANTA (Molecular Simulations) on a Silicon Graphics Indigo workstation. The data were placed into an XPLOR simulated annealing refinement (Brunger et al., 1987) using the structure of uncomplexed isocitrate dehydrogenase as the initial model. XPLOR refinement was performed against the data set from 50 to 2.5 Å resolution. We used a protocol in which the structure, after the initial static energy minimization, is heated to 4000 °C and then immediately placed into a slow cooling (50 ps) annealing minimization. No extended dynamics were performed during the heat stage of the refinement. Sequential cycles of least-squares refinement were run using the same initial model. The *R*-factor was 19.3% after convergence. The structure and a second set of difference maps calculated with new phases from the initial refinement were examined for changes due to the presence of bound isocitrate or its caged precursor, and then the refinements were continued after incorporation of solvent molecules. The final *R*-factor was 18.1% (Table 1).

Flash Photolysis and Turnover in the Crystal. Isocitrate binding to the enzyme active site in the crystal and formation of a productive substrate/cofactor complex after liberation of caged substrate were verified by visible light absorbance spectroscopy studies. A single crystal of IDH, soaked overnight in the dark with 80 mM compound **IV**, magnesium sulfate, and $NADP^+$, was mounted as described above and centered on the X-ray camera. The specimen was flash-irradiated with a focused beam from a 150 W Photomax xenon-arc lamp (Oriel 60137; rhodium intensifiers with Pyrex windows) mated to a beam rotating assembly (Oriel 60130), fast shutter, and bifurcated fiber optic bundle. The total exposure was 2 ms.

Upon binding of isocitrate and magnesium in the presence of $NADP^+$, the initial step of turnover occurs through the transfer of a hydride ion from the C_2 carbon of isocitrate to the nicotinamide ring of $NADP^+$ with an accompanying increase in a broad absorbance peak centered at 340 nm and extending well into the visible absorption range. This signal is easily observable as the production of visible yellow color in the crystal due to the accumulation of bound NADPH in the rate-limiting intermediate complex. The initial binding of isocitrate and subsequent hydride transfer reaction was monitored in the crystal during and after photolysis using a CCD color video camera (Javelin, Inc.) with a 65 mm zoom lens, downloading image frames to a Macintosh LSII workstation with an A/V LG3 Frame Grabber video card (Scion, Inc.; Frederick, MD). The incoming signal to the camera was filtered with a short-pass interference filter (Oriel 58883) to allow only wavelengths below 600 nm to pass through the specimen and to the camera. Use of this spectral range maximizes the signal produced by the production of NADPH, which absorbs in the region 300−500 nm. The body of the crystal was framed and digitized in each image with the software NIH-IMAGE, and the signal was quantitated over time by integration of the total transmittance through the selected area of the crystal over the individual frames, allowing for the monitoring of time-dependent accumulation of reduced nicotinamide in the crystal (Figure 5).

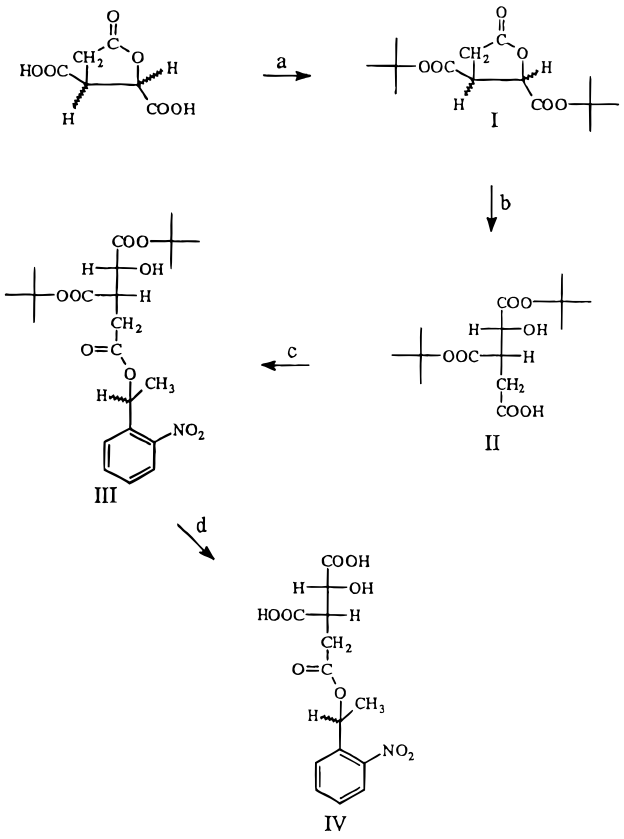

FIGURE 1: Structure and synthesis of caged isocitrate (compound **IV**). Reagents: (a) *t*-BuOH, DCC, DMAP, DMF; (b) NaOH; (c) hydrazone of 2-nitroacetophenone, MnO_2, $CHCl_3$; (d) TFA. The structures shown are only one of the total number of possible diastereomers.

RESULTS

Synthesis

Synthesis of Caged Isocitrate. Photolabile isocitrate (compound **IV**) was synthesized as described in the experimental section and depicted in Figure 1. All intermediates and the final product were characterized by their ^1H NMR spectra and by elemental analysis. High-resolution fast atom bombardment mass spectrometry was also used to confirm the structure of **IV**.

Purity of IV. The final compound (**IV**) (caged isocitrate) was extensively examined for any contamination of reactants, side products, hydrolysis products, or photolysis products by HPLC (data not shown). Using an ion exchange column specifically designed for carboxylic acids, no detectable (lower limit of 100 pmol) contamination was observed as determined by the fact that only one peak was observed by UV detection at 214 and 256 nm. Compound **IV** was especially examined for contaminating isocitrate that could arise from hydrolysis and/or photolysis, using D,L-isocitrate as a standard. No detectable amount of D,L-isocitrate was observed by this analytical method. The lower limit of detectability for D,L-isocitrate was determined to be 100 pmol, which extrapolates to **IV** being at least 90% pure.

There was no attempt made to isolate the biologically active stereoisomer(s) of **IV** nor was there an evaluation

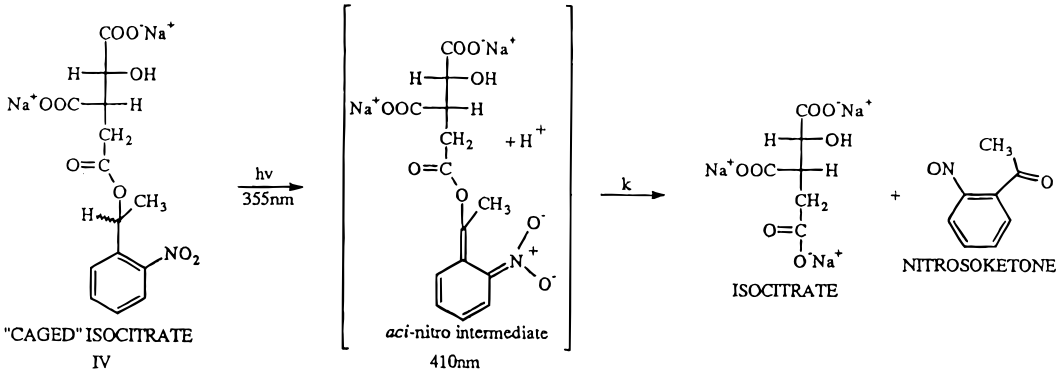

FIGURE 2: The mechanism of photolysis of **IV**. Only one of the possible eight diastereomers is shown.

made on the possible effects of the nonbiological active stereoisomers on the photolysis and subsequent catalytic events.

Biological Activity

Biological Activity in Solution. The biological activity of **IV** as a substrate for IDH was determined in solution. When compared to D,L-isocitrate, **IV** does not exhibit any substrate activity for IDH. The concentration of **IV** was varied over a 1000-fold range from 5 μM to 5 mM, allowing for the possibility that **IV** may be a very poor substrate. The estimation of the purity (contamination by free isocitrate) of **IV** by this assay method is 99.9%.

A second set of experiments to look for very low levels of substrate activity utilized glucose-6-phosphate dehydrogenase in a coupled enzyme assay to look at picomole levels of NADPH. Compound **IV** did not exhibit any substrate activity for IDH as determined by this very sensitive assay. The estimation of the purity (contamination by free isocitrate) of **IV** by this method is 99.95% as established by determining corresponding levels of NADPH.

Laser Pulse Photolysis and Spectroscopy

Quantum Yield. A differential absorption spectrum for the *aci*-nitro intermediate, as formed by pulsed photolysis of **IV** at 355 nm (Figure 2), was recorded in N_2-purged aqueous solution at pH 8 (Tris buffer, 0.1 M). The derived spectrum shows a broad absorption peak centered at 410 nm (Figure 3a). The transient was formed within the 10 ns laser pulse and decayed on a slower time scale. The quantum yield for formation of the *aci*-nitro intermediate (Φ_a) was determined by recording the concentration at the end of the laser pulse as a function of incident laser intensity. Zinc *meso*-tetraphenylporphyrin was used to calibrate the laser intensity. Both solutions were carefully adjusted to possess an absorbance of 0.20 at the excitation wavelength of 355 nm.

Under these conditions,

$$\Phi_a = [\text{ratio}] \times 0.84 \times 74\,000/9100$$

where 0.84 is the quantum yield for the formation of the zinc porphyrin triplet state, 74 000 is the molar extinction coefficient of the porphyrin triplet at 470 nm, and 9100 is the molar extinction coefficient of the *aci*-nitro intermediate at 410 nm. The term [ratio] refers to the ratio of slopes of the absorbance *vs* laser intensity plots for the *aci*-nitro intermediate and porphyrin triplet, respectively. The [ratio] $= 0.044 \pm 0.004$, and therefore, the derived value for Φ_a is 0.30 ± 0.03. As shown by the data in Figure 3b, the quantum yield was essentially independent of pH within the range $4 < \text{pH} > 11$.

Decay Kinetics. The *aci*-nitro derivative was found to decay *via* first-order kinetics with a rate constant of $8.6 \pm 0.9\ s^{-1}$ at pH 8 in deoxygenated aqueous solution (Figure 3c). It was observed that the decay kinetics remained independent of monitoring wavelength within the range of 370−450 nm and of incident laser intensity.

Figure 3d shows the observed effect of pH on the rate constant for decay of the *aci*-nitro intermediate, as monitored at 410 nm. It was observed that the rate of decay, which remained first order at all pH values, increased with decreasing pH throughout the range of $4 < \text{pH} > 9$. Above pH 9, the decay rate remained essentially constant at $2.1 \pm 0.4\ s^{-1}$.

*Energy Quantitation for the Quantitative Conversion of **IV** to Isocitrate.* All of the isocitrate can be released from the **IV** upon laser excitation at 355 nm. Thus, experiments were made with a 2 mL aliquot of solution containing 3.6×10^{-7} mol of **IV** in buffer (0.1 M Tris, pH 7.8). The solution was irradiated with a single laser pulse, and the initial absorbance due to the *aci*-nitro intermediate was measured at 410 nm. This procedure was repeated until no further absorbance change could be observed, and the individual absorbance values were summed. Using the molar extinction coefficient of 9100 $M^{-1}\ cm^{-1}$ at 410 nm for the *aci*-nitro intermediate (Walker et al., 1988), the accumulated absorbance change corresponded to 3.4×10^{-7} mol. Within experimental limits, there was a quantitative conversion, utilizing a total of 40 mJ of energy for the complete release of isocitrate.

*Biological Activity of **IV** upon Photolysis.* To ascertain whether isocitrate was released upon flash photolysis, the laser was pulsed upon a sample of **IV** in the presence of wild-type IDH, Mg^{2+}, and $NADP^+$. The increase in absorbance at 340 nm was monitored following laser excitation (10 ns pulses) at 355 nm after deoxygenation of the solution by purging with N_2. A sample of the same solution not containing IDH was used as a control. The pH was checked after addition of all the ingredients and was found to be 7.81. After laser excitation, absorbance changes were monitored at 340 and at 410 nm. In the absence of IDH, there was an immediate increase in absorbance after the laser pulse (rise time about 10 ns) followed by a slower decrease back to the prepulse base line. The signal at 340 nm was about 10% of that noted at 410 nm, but the kinetics remained identical.

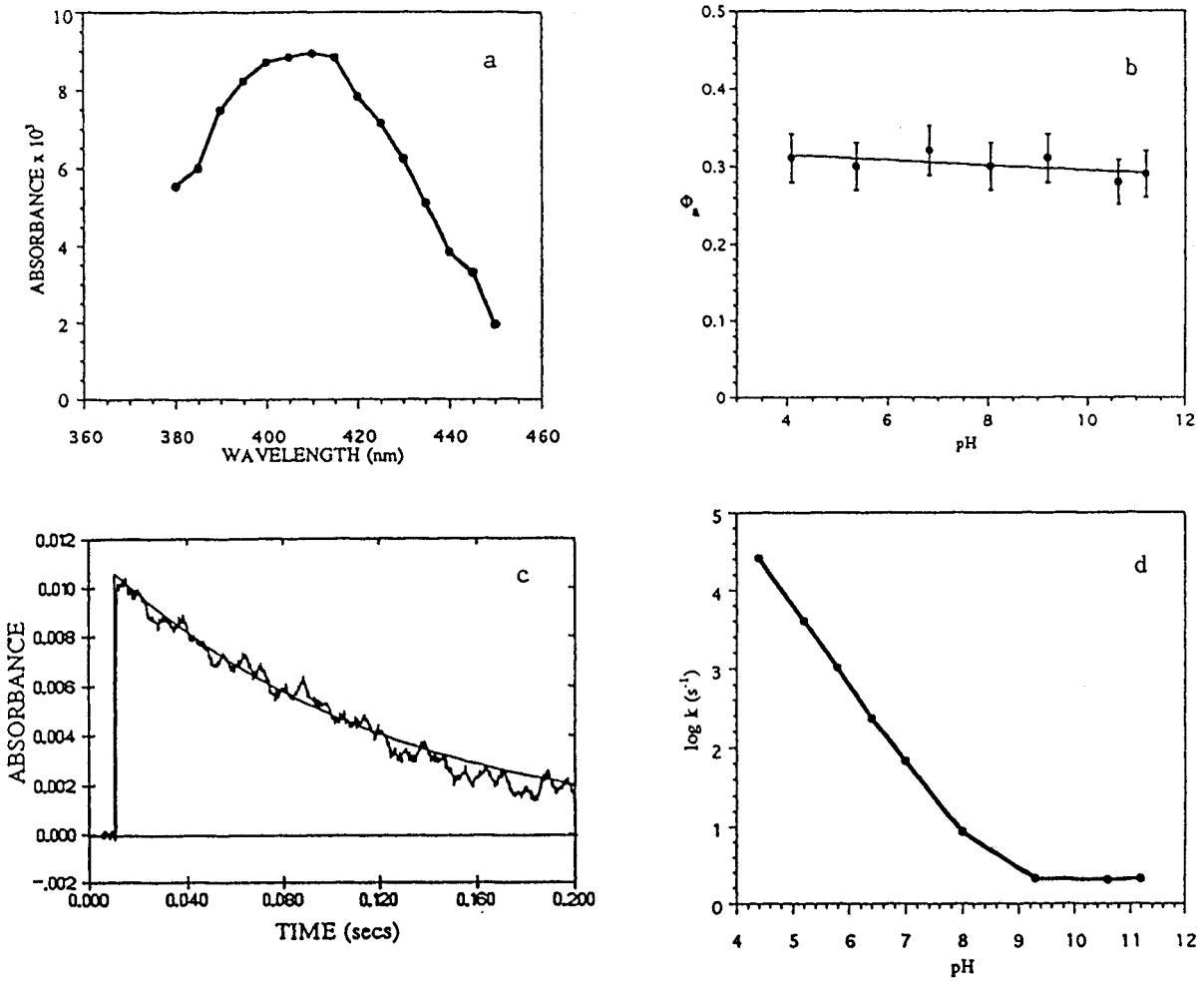

FIGURE 3: Flash photolysis of **IV**. (a) Differential absorption spectrum for the transient *aci*-nitro intermediate as formed by a 10 ns (25 mJ) laser pulse at 355 nm, pH 8. Initial concentration of **IV** was 0.3 mM. (b) Quantum yield (Φ_a) independence of pH. (c) *aci*-Nitro intermediate decay produced by photolysis of 0.3 mM **IV** in 2 mM Tris buffer pH 8, 25 °C. A 10 ns (25 mJ) pulse of laser light at 355 nm initiated the reaction at time zero. The lifetime of the transient was independent of the monitoring wavelength within the range of 370−450 nm and of incident laser intensity. (d) Rate constants for the decay of the transient intermediate in the photolysis of 0.3 mM **IV** as a function of pH measured at 410 nm.

This signal is attributed to the formation and subsequent decay of the *aci*-nitro intermediate. In the presence of IDH, identical behavior was noted at 410 nm but there was an overall increase in absorbance at 340 nm, indicating the formation of a permanent product. This latter change is attributed to the conversion of $NADP^+$ to NADPH, which can only arise from the catalysis of liberated isocitrate by IDH. After computer normalization of the signal at 410 nm, as observed in the absence and presence of IDH, the signal obtained at 340 nm in the absence of IDH was used to correct the base line for the sample containing IDH.

X-ray Crystallography

The Structure of IDH and ***IV*** *and Magnesium before and after Photolysis.* Electron density maps of the enzyme active site prior to photolysis, with Fourier coefficients $[F_{o(\text{soaked crystals, dark})} - F_{o(\text{apoenzyme, wild-type})}]\alpha_{calc}$, calculated with experimentally determined structure factor amplitudes from the enzyme in the dark and computationally derived structure factor amplitudes and phases for wild-type IDH apoenzyme from the Brookhaven Protein Data Base (Hurley et al., 1989), clearly indicate the absence of bound isocitrate at contour levels approaching the noise level of the map (Figure 4A). The maps do, however, show a small (3σ) peak bridging Asp 307 and Asp 311, indicating a low occupancy of bound magnesium ion prior to photolysis. The position of this peak coincides with the metal position in the model of isocitrate and magnesium in complex with the enzyme (Hurley et al., 1990a). No other peaks in the difference map are observed which one could attribute to the binding of isocitrate or its caged precursor.

Difference maps of the enzyme after photolysis, with Fourier coefficients $[F_{o(\text{after photolysis})} - F_{o(\text{before photolysis})}]\alpha_{calc}$, calculated using the experimentally determined structure factor amplitudes from before and after the irradiation of the crystal and initial phases calculated with the coordinates of wild-type apoenzyme (from the Brookhaven PDB as described above), indicate binding of isocitrate and saturation of the enzyme active site (Figure 4B). The maps and refined coordinates for the substrate/metal chelate are isomorphous with previously determined substrate complexes produced through straightforward crystal soaking and cocrystallization experiments (Hurley et al., 1990a; Stoddard et al., 1992a). The largest feature in these maps corresponded to the previously determined position of bound magnesium, with additional density for well-ordered isocitrate substrate bound to the metal and to the surrounding protein side chains. The map agrees with the previously determined wild-type enzyme/

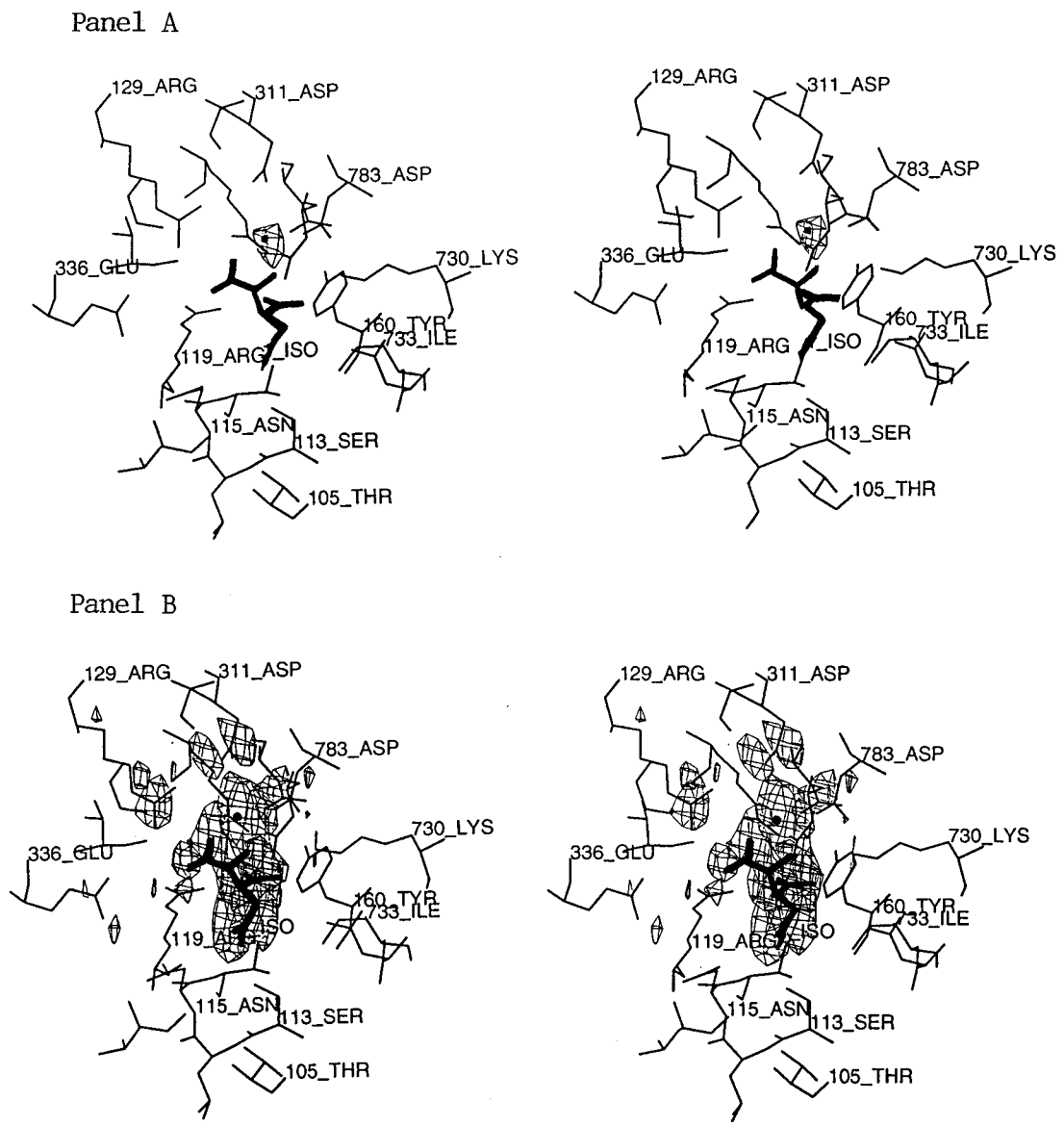

FIGURE 4: Difference Fourier maps of IDH at the active site. Panel A (top) $[F_{o(\text{caged isocitrate/Mg}^{2+}\text{ soak, dark})} - F_{c(\text{apoenzyme})}]\alpha_{calc}$ difference Fourier map calculated for wild-type isocitrate dehydrogenase prior to irradiation. The map was calculated with experimentally determined structure factor amplitudes collected in the dark after soaking the crystal with 80 mM compound **IV** and magnesium sulfate and with structure factors and phases calculated from the coordinates of wild-type apoenzyme from the Brookhaven PDB as described above. An active-site enzyme/substrate complex is not observed prior to photolysis at contour levels approaching the noise level of the map. This result agrees with kinetic data in solution, indicating that the enzyme and caged substrate display no detectable turnover prior to photolysis. The difference density peak shown (contoured at 3σ) is the strongest feature in the map and corresponds to a low occupancy of bound magnesium. The active site residues are shown as thick bonds, and the previously determined model for bound isocitrate (1_ISO) is shown for comparison with the bottom panel. Panel B (bottom). $[F_{o(\text{after photolysis})} - F_{o(\text{dark})}]\alpha_{calc}$ difference Fourier map of the IDH active site. The map was calculated with the experimentally determined structure factor amplitudes, measured both prior to and after photolysis from the same crystal, and initial phases calculated with the coordinates of wild-type apoenzyme from the Brookhaven PDB as described above. The density shown modeled by isocitrate (1_ISO) and magnesium is the strongest feature in the map and indicates binding of isocitrate after liberation from the caged, inactive precursor.

substrate complex (Hurley et al., 1990) about the presence, position, and conformation of the bound binary complex. The final structure after light-induced binding of isocitrate had an *R*-factor of 18.8% and a bond distance root-mean square of 0.023 Å from ideality. The occupancies of the bound substrate and metal were fixed at unity during the refinement, and their individual atomic temperature factors were allowed to refine independently. The values of these *B*-factors ranged from 20 to 30 Å^2 and are comparable to the surrounding protein side chains in the active site, indicating that the assignment of the bound ternary complex is correct. The results of the final refinement are shown in Table 1. Difference maps of the enzyme after irradiation clearly indicate that the metal/substrate chelate binds in the same relative position and orientation as in the wild-type enzyme. The largest difference is in the bound metal, which is displaced by slightly less than 0.2 Å from the magnesium site in the wild-type structure. The metal is easily modeled in the strongest peak in the $[F_{o(\text{after photolysis})} - F_{o(\text{dark})}]$ difference map (Figure 4B). The bound isocitrate is located in the same position and orientation as in the wild-type complex, with all specific interactions to the active site side chains isomorphous with the wild-type enzyme/substrate complex. No density was observed for unphotolyzed nitrobenzyl groups still bound to the enzyme-associated isocitrate molecules.

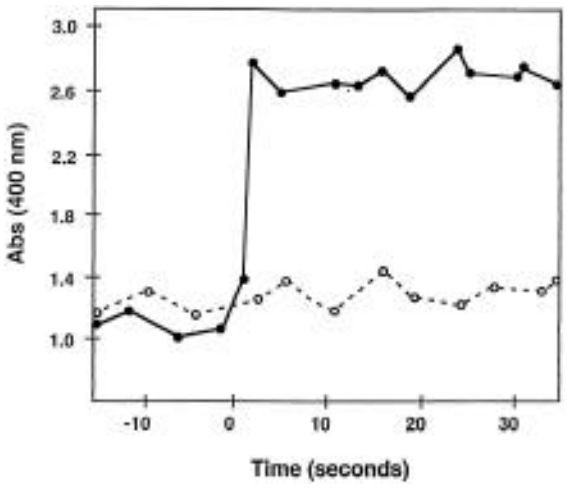

FIGURE 5: Single-crystal absorbance measurements of substrate binding. Using flash photolysis of **IV** (solid thick line with dark spheres), 80 mM isocitrate and Mg^{2+} was presented to the crystal. In order to assay substrate binding through the enzymatic dehydrogenation of bound isocitrate and reduction of the nicotinamide ring of the cofactor, 50 mM $NADP^+$ was also included. The molar absorptivity of crystalline protein, caged isocitrate, and $NADP^+$ at these concentrations is sufficiently low over the wavelength range of photoactivation induced by the arc lamp (400−600 nm after prefiltering of the flash; ϵ less than 0.01 μmol^{-1} L cm^{-1}) that photoisomerization appears to be spatially uniform through the volume of the crystal. This is supported by the high-saturating absorbance signal measured upon flash photolysis of the caged isocitrate in the presence of $NADP^+$, in response to light-triggered enzymatic catalysis of hydride transfer and reduction of $NADP^+$. In addition, the high-occupancy isocitrate−Mg^{2+} complex observed crystallographically upon flash photolysis under these conditions indicates uniform, efficient liberation of free isocitrate. The strong absorbance signal from the crystal during formation of NADPH in the crystal lattice clearly leads to saturation of the detector in the experiment as shown. For time-resloved Laue experiments, the input wavelength range to the absorbance detector (single-crystal microspectrophotometer or CCD visible detector) should be appropriately truncated to allow accurate determination of binding and turnover while still maintaining linearity of response. The dashed line (with open spheres) shows a control experiment with 50 mM Mg^{2+} and $NADP^+$, but no isocitrate, demonstrating that the increased signal upon photolysis is induced by the binding of free isocitrate in the active site.

Substrate Binding in the Crystal Studied by Visible Light Absorbance. The time-dependent production of reduced NADPH in the crystal, caused by transfer of a hydride ion from bound isocitrate to the C_4 carbon of the $NADP^+$ nicotinamide ring during the first step in catalysis after formation of the ternary Michaelis complex, was measured by visible light absorbance as described in the methods section. At the very high concentration of enzyme and bound $NADP^+$ found in the crystal (5 mM), reduction of the cofactor is accompanied by a visible, measurable increase in color within the crystal in the yellow portion of the visible spectrum. The experiment was performed by introducing the substrate by flash photolysis of **IV**. Wild-type IDH was assayed for substrate binding and hydride transfer which has a maximum k_{cat} of 76 s^{-1}.

As shown in Figure 5, after flash photolysis and isocitrate release, wild-type IDH crystals displayed an increase in absorbance in the visible spectrum (350−500 nm) caused by the increased absorbance of the newly reduced NADPH cofactor in the crystal (which absorbs with a maximum peak at 340 nm and a broad absorbance shoulder and tail which extend into the region monitored in this study). This increase in absorbance and consequent decrease in transmittance by the crystal is accompanied by an observable accumulation of colored product in the crystal. The wild-type enzyme in the crystal appears to complete its transition to a new base line within the fastest resolution of the experiment (0.1 s), indicating complete binding and hydride transfer within that time period. As a negative control, crystals soaked with caged substrate and NADP cofactor in the absence of Mg^{2+}, or with NADP alone, were not observed to accumulate reduced NADPH upon photolysis, indicating that the light-driven liberation of substrate specifically induces turnover in the crystal.

DISCUSSION

In order to determine the crystallographic structure of a catalytic intermediate formed during enzymatic turnover, a method must be found to induce the homogenous accumulation of that species throughout the volume of the crystal, during which time diffraction data may be collected, usually using the polychromatic X-ray beam produced at an X-ray synchrotron (often referred to as the Laue technique). The most common approach currently under development for a large number of systems is the use of photolabile, nonreactive caged substrates or cofactor analogues, such as calcium-nitrophen, 2-nitrobenzyl-ATP, and the photolabile isocitrate trigger described here. In order to use such a photochemical trigger successfully to induce an initial sychronized round of turnover in the crystal, a number of criteria must be met:

(i) The caged compound must be completely catalytically inert and unreactive prior to photolysis.

(ii) The caged compound must be soluble in the crystallization mother liquor and in the solvent-filled interstices of the crystal to a concentration at least 1 order of magnitude above the crystalline enzyme concentration (approximately 5 mM) and above the apparent binding constant K_m in the presence of the crystallization mother liquor.

(iii) The half-life of the excited species formed upon photon absorption must be significantly shorter than the half-life of any rate-limited catalytic species which accumulates transiently upon substrate binding during the first round of turnover.

(iv) The caged compound must exhibit a highly efficient absorption of photons and release of substrate upon photolysis, in order to induce a fast increase in available substrate during the time course of a single short light pulse. The well-ordered crystal lattice must also be preserved during this photolytic event.

(v) The rate of all binding events which occur between the photolytic reaction and formation of the Michaelis complex must be substantially faster than the rate of decay of the intermediate complex under study.

A photolabile isocitrate derivative was synthesized and has the potential (by satisfying the criteria outlined above) to be used in combination with Laue X-ray crystallography techniques for the real-time observation of catalytic intermediate(s) arising from the catalysis of isocitrate to α-ketoglutarate by isocitrate dehydrogenase. Photolabile caged isocitrate (compound **IV**) has been examined in detail to ascertain whether it meets the necessary criteria listed above.

Careful analysis by two different methods indicates no measurable reduction of $NADP^+$ by the enzyme prior to flash photolysis and demonstrates that in solution the caged

cofactor is completely inert in the enzyme active site and that the conditions (criteria i and ii) for pre-steady-state initiation of turnover are met.

In addition to characterizing **IV** in solution, single-crystal UV spectroscopy and monochromatic diffraction analysis have been used to assay the reactivity and structural interactions of **IV** in the crystal before and after photolysis. When the crystal was assayed for reduction of cofactor and reflection intensities of the crystal before and after photolysis were monitored, no substrate activity was observed, which further illustrates that **IV** is completely catalytically inert prior to photolysis.

Compound **IV**, which is a dicarboxylic acid, is very soluble in aqueous solutions provided the pH value is above the pK_a values of the acidic groups. The 2-nitrobenzyl moiety of **IV** presented some difficulty solubilizing the compound in crystallization mother liquor (40% saturated ammonium sulfate). This difficulty was overcome by predilution of the compound in high-concentration buffers with an elevated pH and/or addition of small amounts of an organic water miscible solvent.

The actual rate and efficiency of liberation of free substrate upon irradiation have been measured. Fast kinetic measurements of the rate of liberation of the 2-nitrobenzyl leaving group from isocitrate, carried out in a similar manner to the direct measurement of the rate of cinnamate lactonization upon photolysis (Stoddard et al., 1990), have provided an accurate estimate of the lifetime of the excited species upon light absorption, of the time necessary for full conversion of caged cofactor in the crystal, and of the quantum efficiency or yield of the photolysis reaction. Using these values, we can estimate the intensity and flash duration necessary for full photolytic triggering. Since the light-sensitive 2-nitrobenzyl caging group has already been well characterized with a number of other organic moieties, is known to possess an extremely high quantum efficiency, and has been used as a triggering group in past Laue studies (Schlichting et al., 1989; Duke et al., 1992), it is not surprising that the compound described here possesses sufficient photoreactivity to serve as a catalytic trigger.

A spectral intermediate was observed upon laser pulse photolysis of **IV** (caged isocitrate), which was analogous to the presumed *aci*-nitro intermediate observed for the photolysis of 2-nitrobenzyl caged nucleotides (McCray et al., 1980). By measurement of the absorbance and study of the time dependence of the disappearance of the *aci*-nitro intermediate, details concerning the photolytic reaction process such as quantum yield (Milburn et al., 1989) and kinetics were determined.

Information about whether isocitrate could be released quantitatively was addressed by quantifying the amount of the *aci*-nitro intermediate formed. Upon illumination of a sample of **IV** in buffered solution, quantitative conversion to isocitrate could be achieved. To ensure that isocitrate was being released upon the decay of the *aci*-nitro intermediate, the same experiment was performed in the presence of IDH and the necessary cofactors in buffered solution. Upon pulsed photolysis of caged isocitrate, the liberated isocitrate was enzymatically converted to α-ketoglutarate as observed by the spectral formation of NADPH.

The quantum yield was determined by observing the accumulation of the *aci*-nitro intermediate. The quantum yield for the formation of the *aci*-nitro intermediate was determined by measuring the concentration (using a previously published extinction coefficient (McCray & Trentham, 1989)) as a function of laser intensity. Well-established methods were used to calibrate laser intensity. The quantum yield was determined to be 0.3, which is comparable to the range of quantum yield values (0.003−0.63) reported for 2-nitrobenzyl caged nucleotides (Wooton & Trentham, 1989). The quantum yield was independent of pH within experimental error (Figure 3b). Additional studies indicate that approximately 1 mJ of energy at 355 nm is necessary to quantitatively convert 1 μmol of caged compound to free isocitrate. Assuming that in an actual time-resolved crystallographic experiment a crystal volume of 1 μL (1 mm^3) is loaded with 10 mM compound **IV**, then a fully efficient, quantitative conversion to 10 mM isocitrate in the crystal would involve the light-driven release of 1×10^{-2} μmol of compound, necessitating the input of a minimum of 1×10^{-2} mJ of light at 355 nm, over a time period of photolysis of less than 1 ms. Such values for energy input and exposure times are easily achieved with a variety of lasers or Xe-Hg flash lamps with fast shutter assemblies. In addition, our studies on crystalline IDH indicate that the crystal lattice is capable of withstanding substantially higher fluxes of light at this wavelength.

The rate of release of isocitrate was determined by measuring the rate of decay of the *aci*-nitro intermediate. The *aci*-nitro intermediate exhibited first-order decay kinetics as illustrated in Figure 3c. The rate of decay of the *aci*-nitro intermediate (release of isocitrate) was dependent on the pH of the buffered solution. The rate of isocitrate release increased with decreasing pH throughout the range of 4−9 (Figure 3d). The rate at pH 4 was determined to be 25 900 s^{-1} and decreases to 2 s^{-1} at pH 9, with half-lives of 0.027 and 347 ms, respectively. The rate of decay at neutral pH was determined to be 67.3 s^{-1} with a half-life of 10 ms, which is comparable to the values for 2-nitrobenzyl ATP (decay rates of 18−84 s^{-1}, half-lives of 39−8 ms, respectively), but the *aci*-nitro intermediate exhibits a slower decay rate and longer half-life than does 2-nitrobenzyl caged phosphate (decay rates of 21000−80000 s^{-1}, half-lives of 33−9 μs, respectively) (Wootton & Trentham, 1989). The dependence of the rate on hydrogen ion concentration has also been observed with other 2-nitrobenzyl caged biomolecules, further illustrating that the mechanism of isocitrate release is presumably the same as that for 2-nitrobenzyl caged nucleotides (McCray & Trentham, 1989).

For wild-type isocitrate dehydrogenase at optimal pH (approximately 7.8), the turnover rate is approximately 56 s^{-1}, which gives a half-life for the rate-limited catalytic species of approximately 9 ms, assuming that the rate limit for the enzyme is caused by a single predominant energetic barrier in the overall reaction pathway. At a slightly lower pH of 6.5, this half-life is approximately doubled to 20 ms. The caged isocitrate trigger displays a sharp increase in rate of release as a function of decreasing pH, with a rate of 8.6 s^{-1} at pH 8.0 (giving a half-life of the *aci*-nitro intermediate of 81 ms), increasing to 234 s^{-1} (half-life of 3 ms) at pH 6.5. Therefore, the trigger displays a pH rate profile under slightly acidic conditions (pH 6−7) which is sufficiently fast to drive the homogenous accumulation of a catalytic intermediate which possesses a half-life of 10−20 ms under the same conditions.

ACKNOWLEDGMENT

The authors acknowledge Dr. Anthony Harriman at the Center for Fast Kinetics, University of Texas at Austin, for performing the flash photolysis experiments and analysis of the data.

REFERENCES

Adams, S. R., & Tsien, R. Y. (1993) *Annu. Rev. Physiol. 55*, 755−784.
Bernofsky, C., & Swan, M. (1973) *Anal. Biochem. 53*, 452−458.
Bernstein, F. C., Koetzle, T. F., Williams, G. J. B., Meyer, E. F., Jr., Brice, M. D., Rodgers, J. R., Kennard, O., Shimanouchi, T., & Tasumi, M. (1977) *J. Mol. Biol. 112*, 535−542.
Bolduc, et al. (1995) The Use of Mutagenesis and Laue Crystallography to Examine the Intermediates in a Reaction Pathway: Isocitrate dehydrogenase, *Science 268*, 1312−1318.
Brunger, A. T., Kuriyan, J., & Karplus, M. (1987) *Science 235*, 458.
Corrie, J. E. T., & Trentham, D. R. (1993) *Bioorg. Photochem. 2*, 243−305.
Cruikshank, D. W. J., Helliwell, J. R., & Johnson, L. N. (1992) *Philos. Trans. R. Soc. London, Ser. A 340*, 169.
Dean, A. M., & Koshland, D. E., Jr. (1990) *Science 249*, 1044−1046.
Dean, A. M., & Koshland, D. E., Jr. (1993) *Biochemistry 32*, 9302−9308.
Duke, E. M. H., Hadfield, A., Walters, S., Wakatsuki, S., Bryan, R. K., & Johnson, L. N. (1992) *Philos. Trans. R. Soc. London, Ser. A 340*, 245−261.
Gurney, A. M., & Lester, H. A. (1987) *Physiol. Rev. 67*, 583.
Hadfield, A., & Hajdu, J. (1994) *J. Appl. Crystallogr. 26*, 839−842.
Hajdu, J., & Johnson, L. N. (1990) *Biochemistry 29*, 1669−1678.
Hurley, J. H., Thorsness, P. E., Ramalingam, V., Helmers, N. H., Koshland, D. E., Jr., & Stroud, R. M. (1989) *Proc. Natl. Acad. Sci. U.S.A. 86*, 8635−8639.
Hurley, J. H., Dean, A. M., Sohl, J. L., Koshland, D. E., Jr., & Stroud, R. M. (1990a) *Science 249*, 1012−1016.
Hurley, J. H., Dean, A. M., Thorsness, P. E., Koshland, D. E., Jr., & Stroud, R. M. (1990b) *J. Biol. Chem. 265*, 3599.
Hurley, J. H., Dean, A. M., Koshland, D. E., Jr., & Stroud, R. M. (1991) *Biochemistry 30*, 8671−8678.
Hurley, J. K., Sinai, N., & Linschitz, H. (1983) *Photochem. Photobiol. 38*, 9.
Jones, T. A. (1978) *J. Appl. Crystallogr. 11*, 268−272.
McCray, J. A., & Trentham, D. R. (1989) *Annu. Rev. Biophys. Biophys. Chem. 18*, 239−270.
Milburn, T., Matsubara, N., Billington, A. P., Udgaonkar, J. B., Walker, J. W., Carpenter, B. K., Webb, W. W., Marque, J., Denk, W., McCray, J. A., & Hess, G. P. (1989) *Biochemistry 28*, 49−55.
Moffat, K. (1989) *Annu. Rev. Biophys. Biophys. Chem. 18*, 309−332.
Nisselbaum, J. S., & Green S. (1969) *Anal. Biochem. 27*, 212−217.
Pekkarinen, L., & Linschitz, H. (1960) *J. Am. Chem. Soc. 82*, 2407.
Schlichting, I., Rapp, G., John, J., Wittinghofer, A., Pai, E. F., & Goody, R. S. (1989) *Proc. Natl. Acad. Sci. U.S.A. 86*, 7687−7690.
Stoddard, B. L., Koenigs, P., Porter, N., Petratos, K., Petsko, G. A., & Ringe, D. (1991) *Proc. Natl. Acad. Sci. U.S.A. 88*, 5503−5507.
Stoddard, B. L., & Koshland, D. E., Jr. (1993) *Biochemistry 32*, 9317−9322.
Stoddard, B. L., Dean, A., & Koshland, D. E. (1993) *Biochemistry 32*, 9310−9316.
Stryer, L. (1988) *Biochemistry*, p 375, Freeman & Co., New York.
Walker, J. W., Reid, G. P., McCray, J. A., & Trentham, D. R. (1988) *J. Am. Chem. Soc. 110*, 7170.
Wootton, J. F., & Trentham, D. R. (1989) in *Photochemical Probes in Biochemistry* (Nielsen, P. E., Ed.) pp 277−296, Kluwer Academic Publishers, Dordrecht, The Netherlands.

BI951105V